Supporting Information

Electrochemical Dehydrogenation of Ethane to Ethylene in a Solid Oxide Electrolyser

Xirui Zhang[1], Lingting Ye[1], Hao Li[1], Fanglin Chen[2], Kui Xie[1,*]

[1] Key Laboratory of Design and Assembly of Functional Nanostructures, Fujian Institute of Research on the Structure of Matter, Chinese Academy of Sciences, Fuzhou, Fujian 350002, China.

[2] Department of Mechanical Engineering, University of South Carolina, 300 Main Street, Columbia, SC 29208, USA.

* Corresponding Author's E-mail: kxie@fjirsm.ac.cn

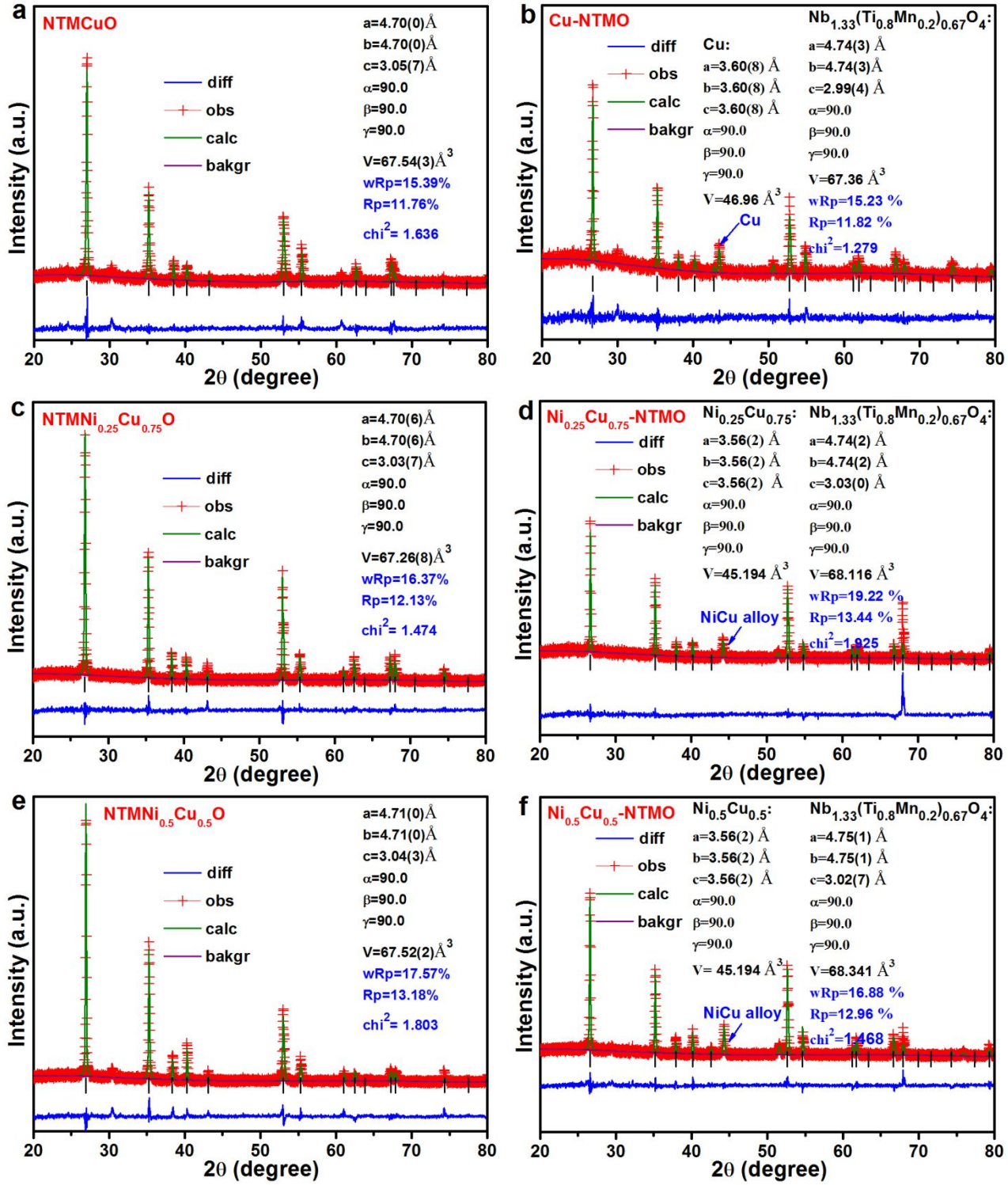

Figure S1. XRD rietveld refinement patterns of (a) oxidized NTMCuO; (b) reduced Cu-NTMO; (c) oxidized $NTMNi_{0.25}Cu_{0.75}O$; (d) reduced $Ni_{0.25}Cu_{0.75}$-NTMO; (e) oxidized $NTMNi_{0.5}Cu_{0.5}O$; (f) reduced $Ni_{0.5}Cu_{0.5}$-NTMO.

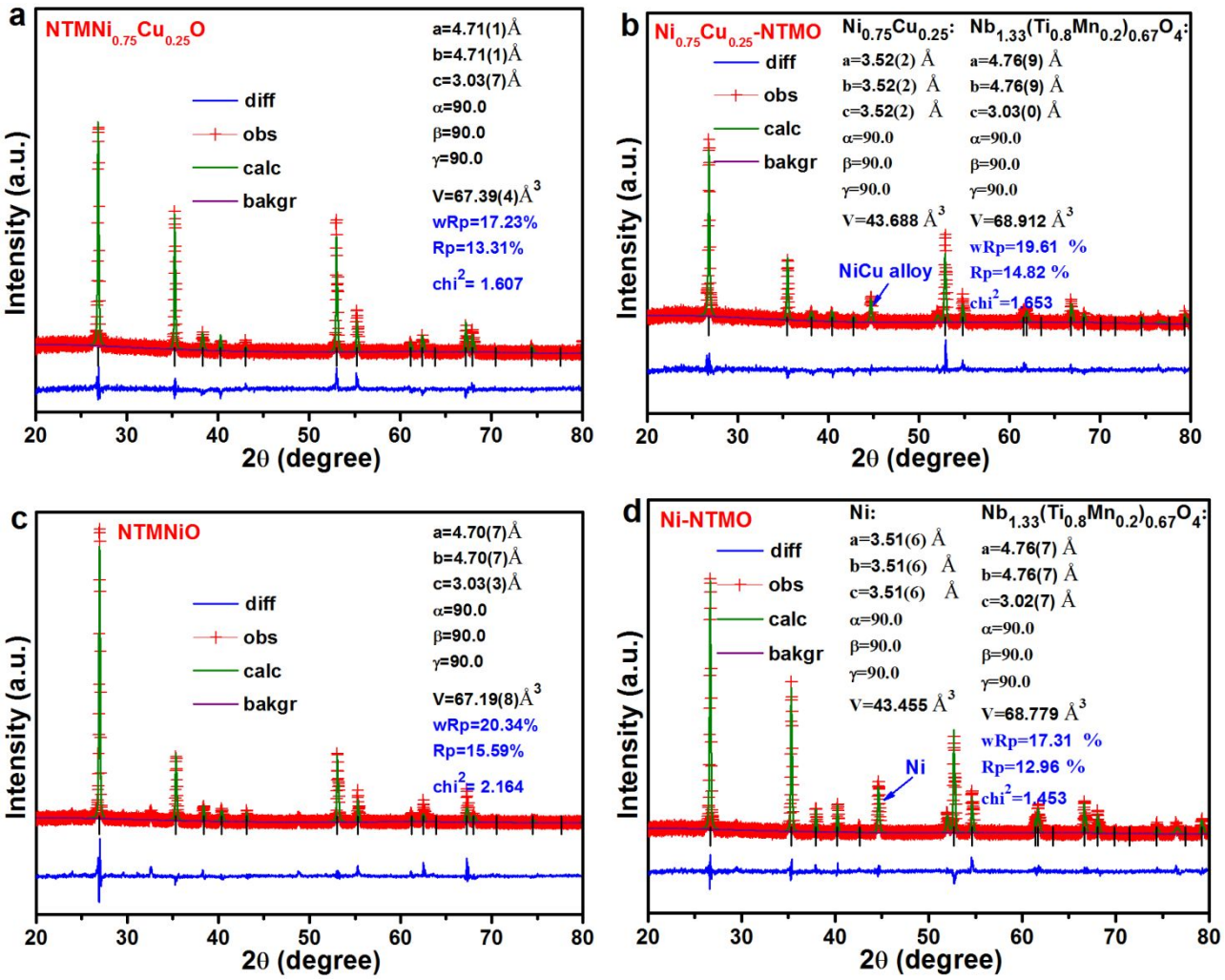

Figure S2. XRD rietveld refinement patterns of (a) oxidized NTMN$i_{0.75}Cu_{0.25}O$; (b) reduced $Ni_{0.75}Cu_{0.25}$-NTMO; (c) oxidized NTMNiO; (d) reduced Ni-NTMO.

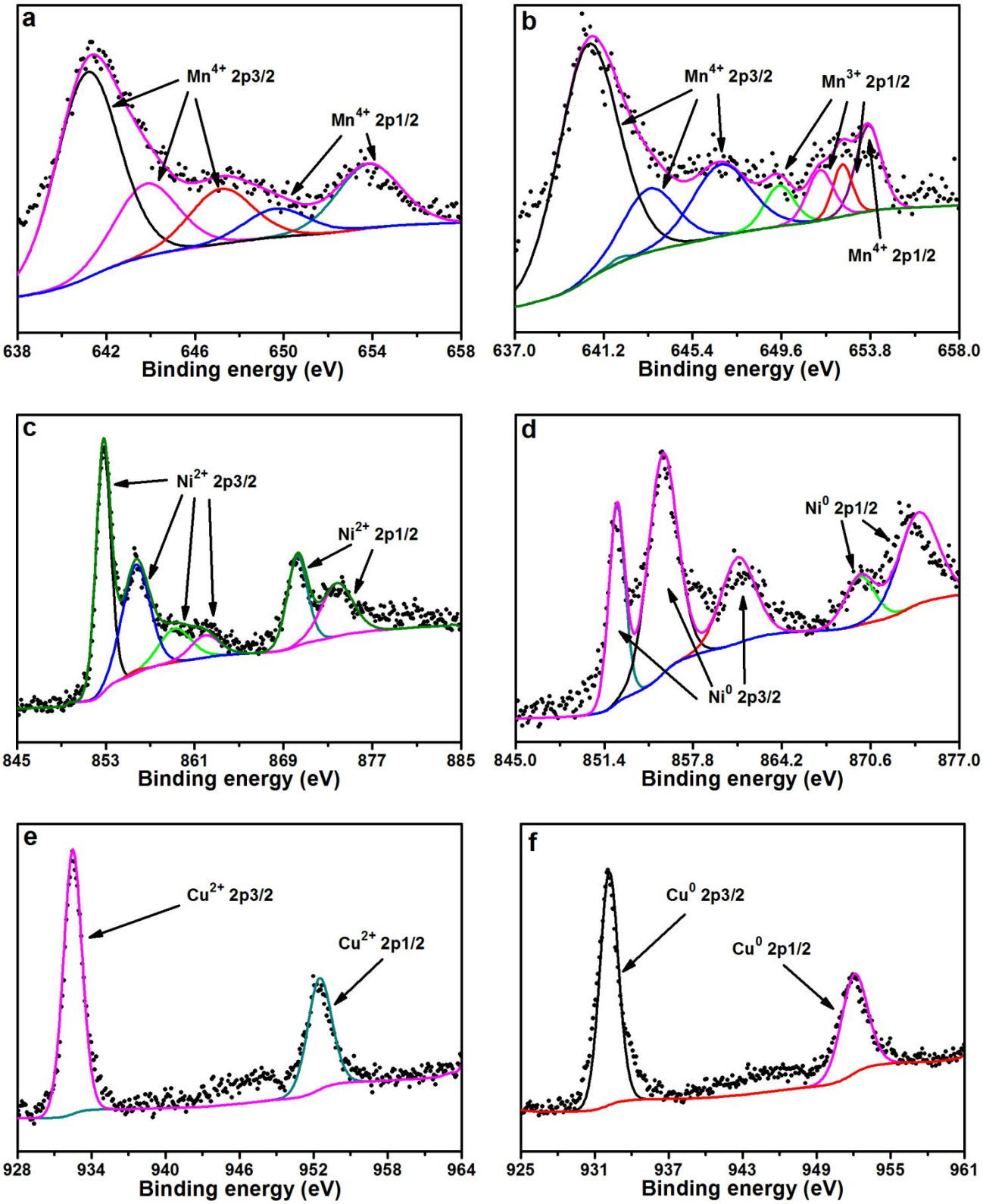

Figure S3. X-ray photoelectron spectroscopy of (a) Mn, (c) Ni, (e) Cu in the oxidized NTM$Ni_{0.5}Cu_{0.5}O$; (b) Mn, (d) Ni, (f) Cu in the reduced $Ni_{0.5}Cu_{0.5}$-NTMO.

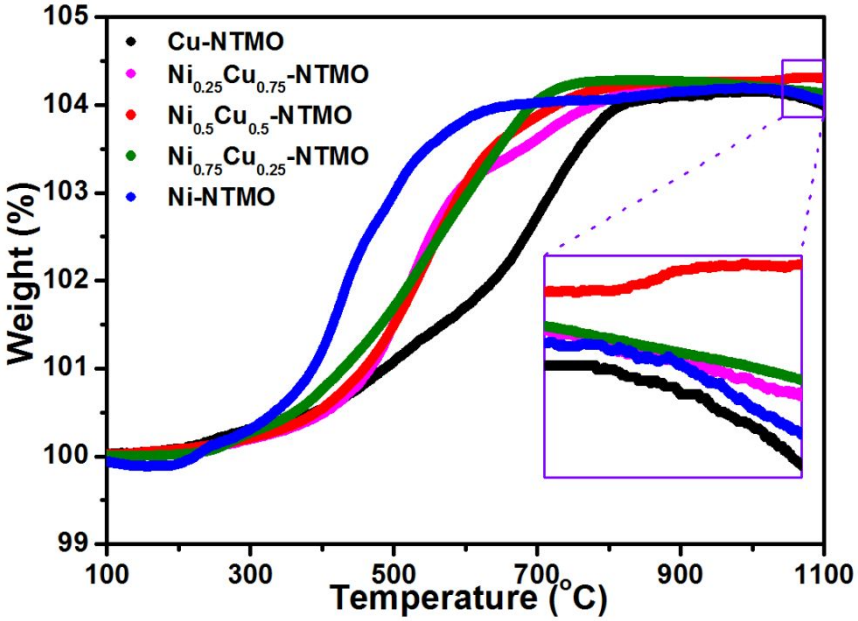

Figure S4. TGA tests of the reduced samples from 100 to 1100 ˚C in air.

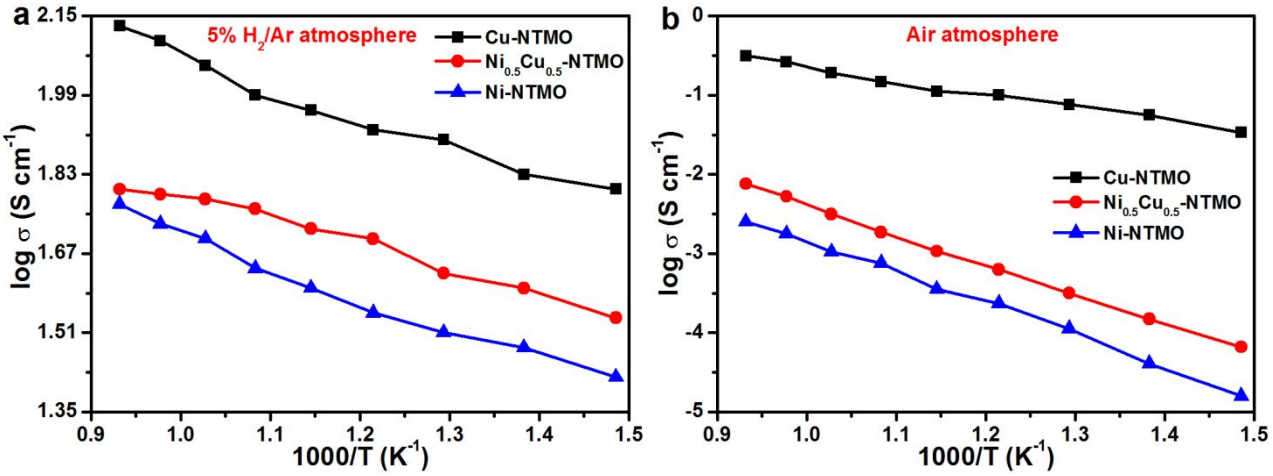

Figure S5. The dependence of mixed conductivity on temperature of the reduced samples in (a) 5% H_2/Ar and (b) air atmosphere.

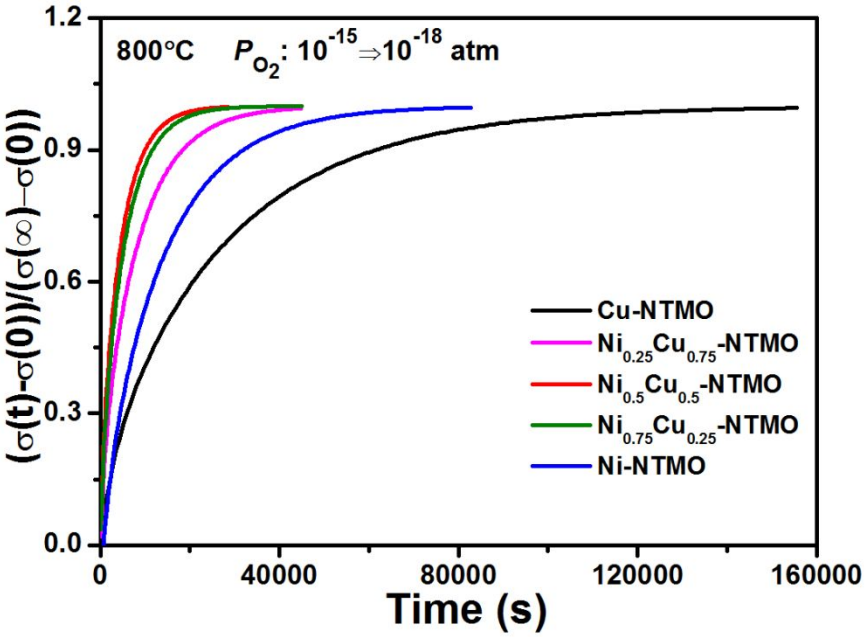

Figure S6. Oxygen exchange coefficient diagram of the reduced samples.

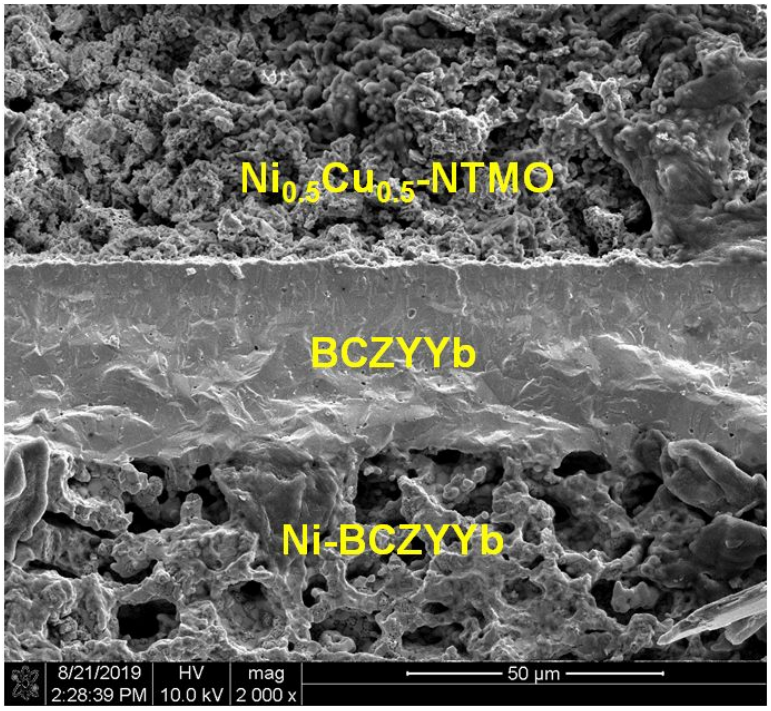

Figure S7. Cross sectional microstrucutre of a solid oxide electrolyser with a configuration of $Ni_{0.5}Cu_{0.5}$-NTMO-SDC|BCZYYb|Ni-BCZYYb before test.

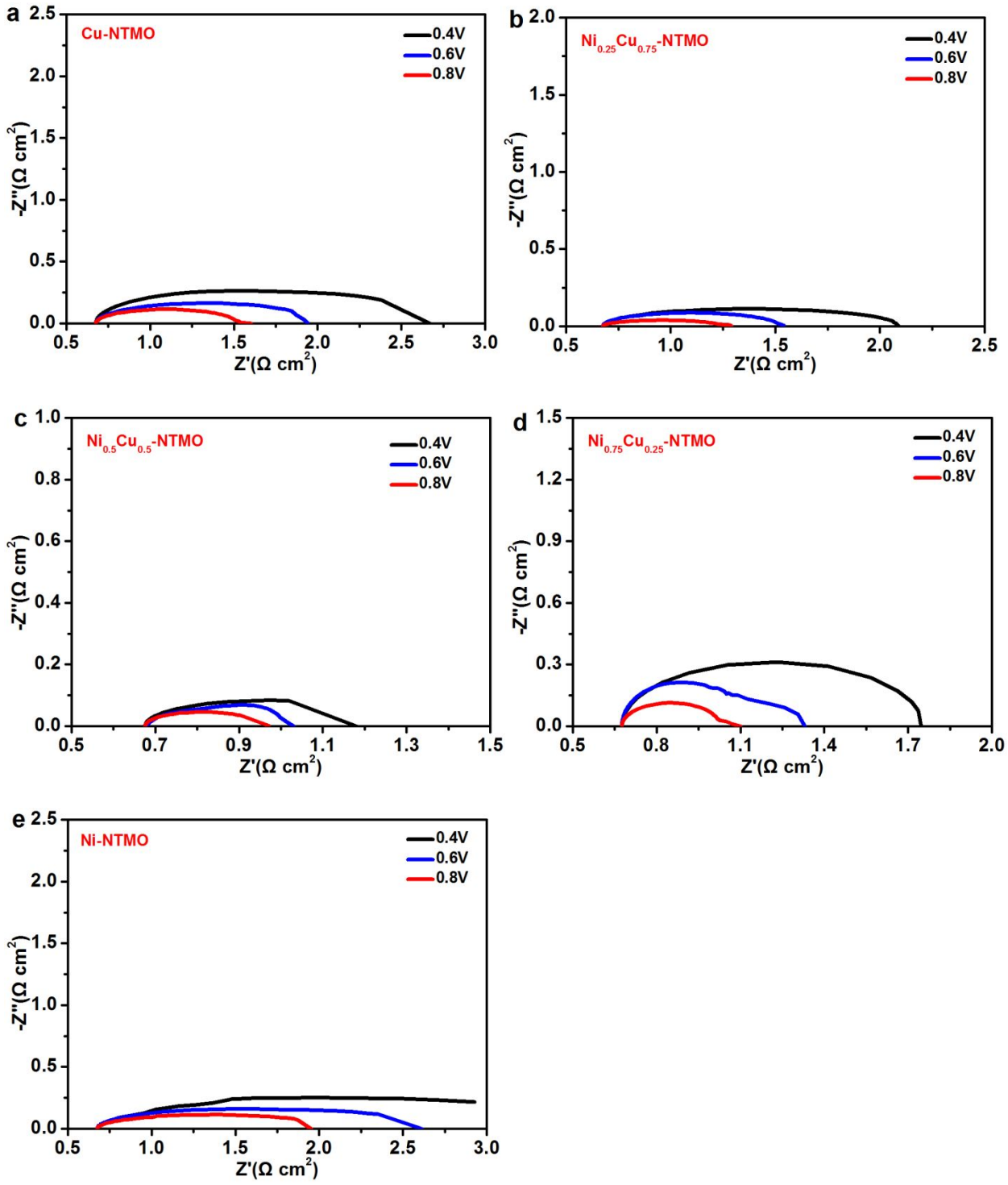

Figure S8. AC impedance of solid oxide electrolysers based on (a) Cu-NTMO, (b) $Ni_{0.25}Cu_{0.75}$-NTMO, (c) $Ni_{0.5}Cu_{0.5}$-NTMO, (d) $Ni_{0.75}Cu_{0.25}$-NTMO, (e) Ni-NTMO anodes under various potentials at 700 ˚C.

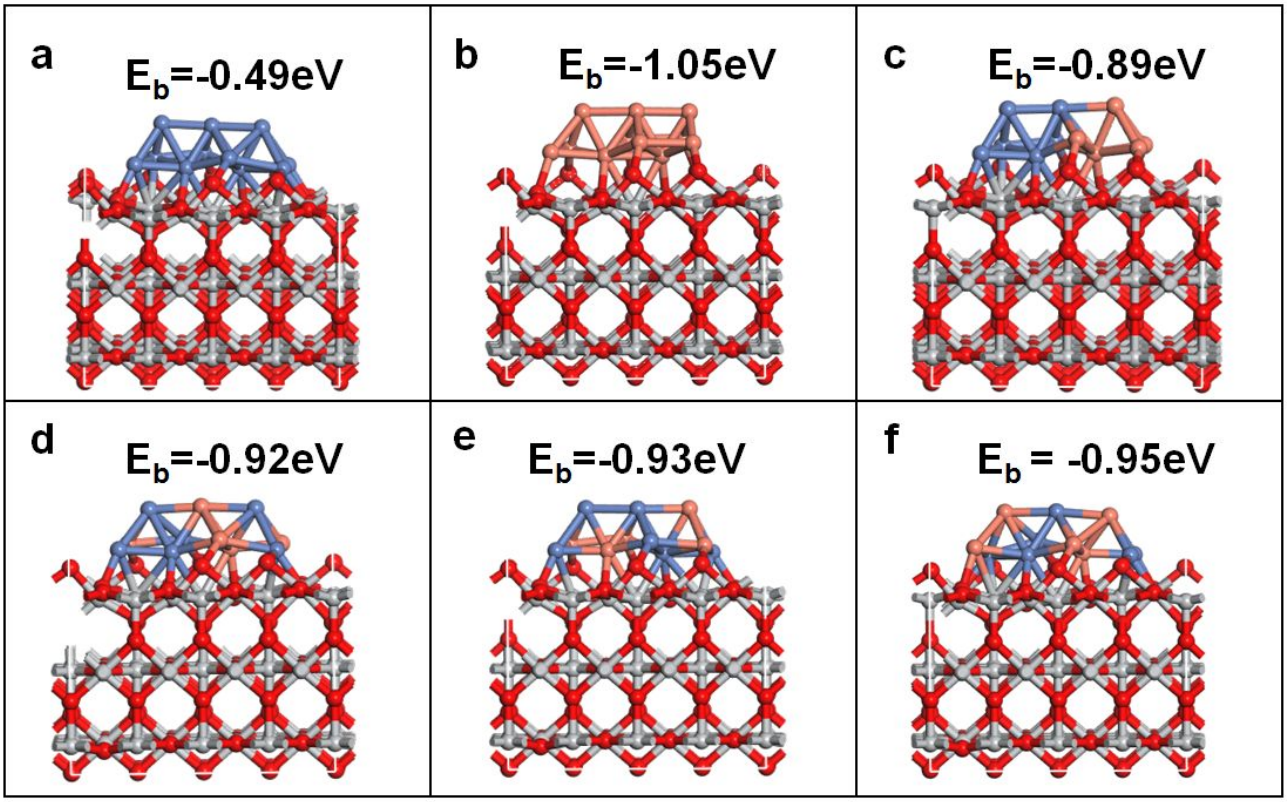

Figure S9. Optimization structure and binding energy of clusters. (a) Ni11 cluster; (b) Cu11 cluster; (c) (Ni-Cu)-1 cluster; (d) (Ni-Cu)-2 cluster; (e) (Ni-Cu)-3 cluster ; (f) (Ni-Cu)-4 cluster. (copper in orange, nickel in bule, titanium in silver white, oxygen in red)

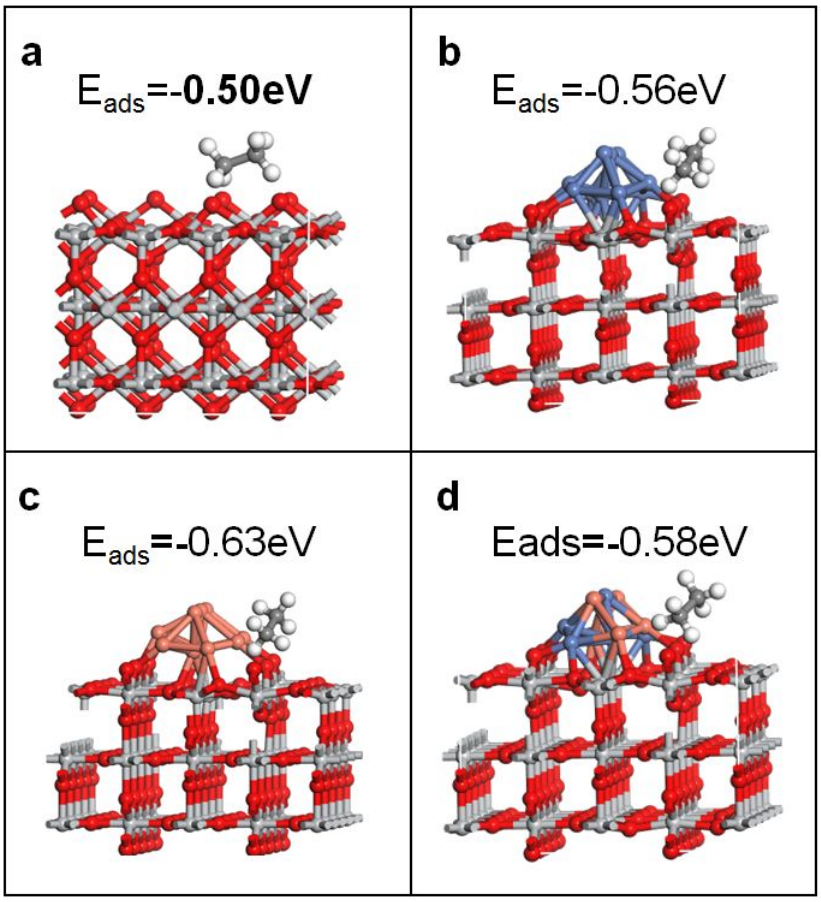

Figure S10. Different adsorption configurations of ethane on the TiO_2 system. (a) The defect surface; (b) The Ni/TiO_2 system; (c) The Cu/TiO_2 system; (d) The Ni-Cu/TiO_2 system. (carbon in gray, copper in orange, nickel in bule, titanium in silver white, oxygen in red and hydrogen in white)

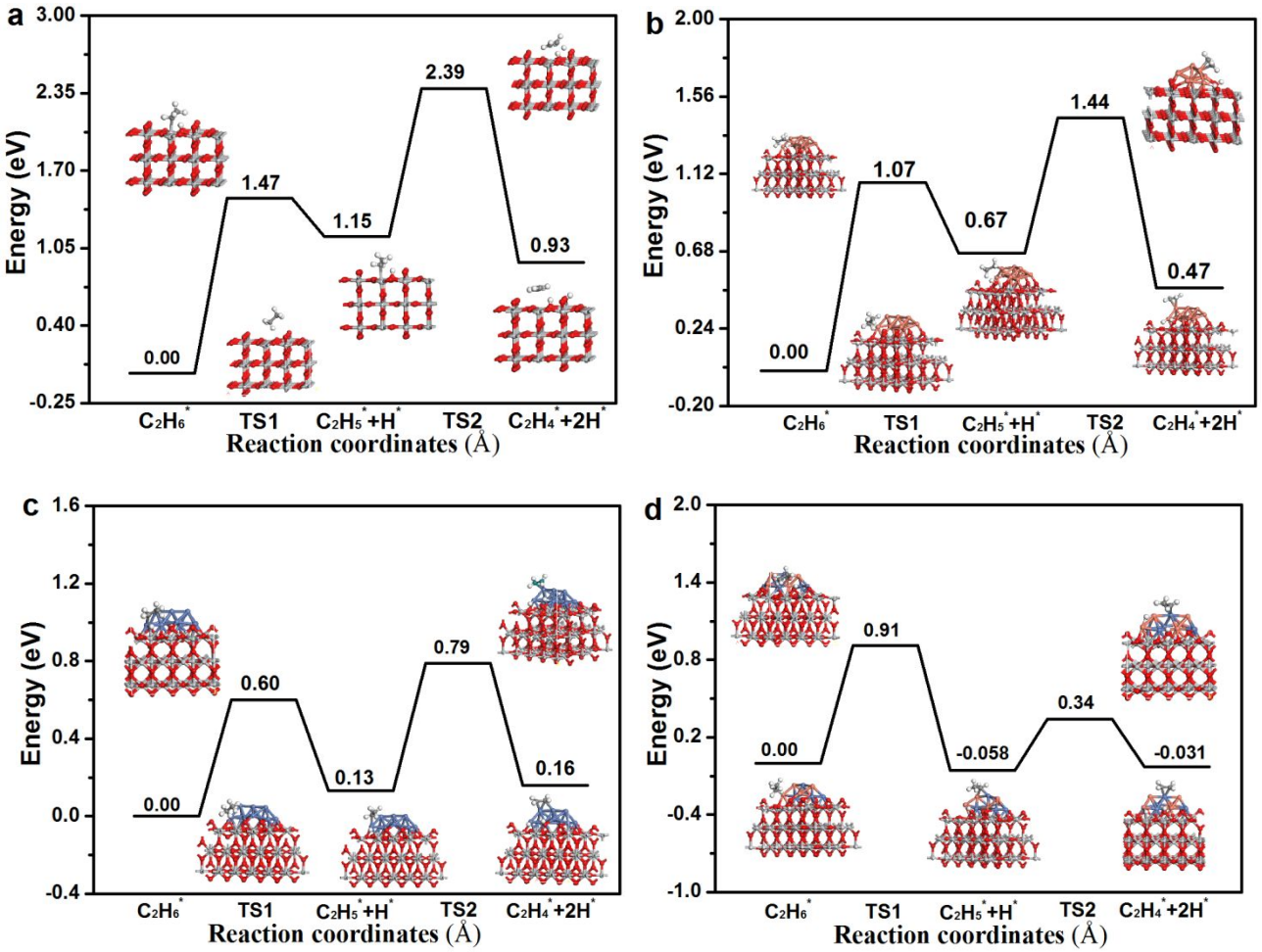

Figure S11. Potential energy profile for the ethane dehydrogenation on (a) TiO_2 defect surface, (b) Cu/TiO_2 interface, (c) Ni/TiO_2 interface and (d) $NiCu/TiO_2$ interface. (carbon in gray, copper in orange, nickel in bule, titanium in silver white, oxygen in red and hydrogen in white)

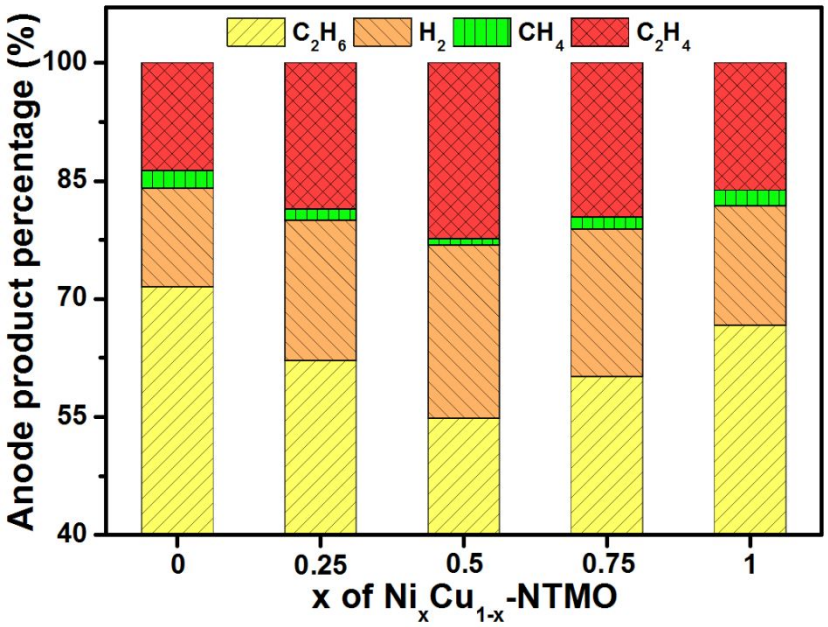

Figure S12. The product analysis from thermal splitting C_2H_6 in the anode of solid oxide electrolyser without externally applied voltages at operation temperature of 700 ˚C.

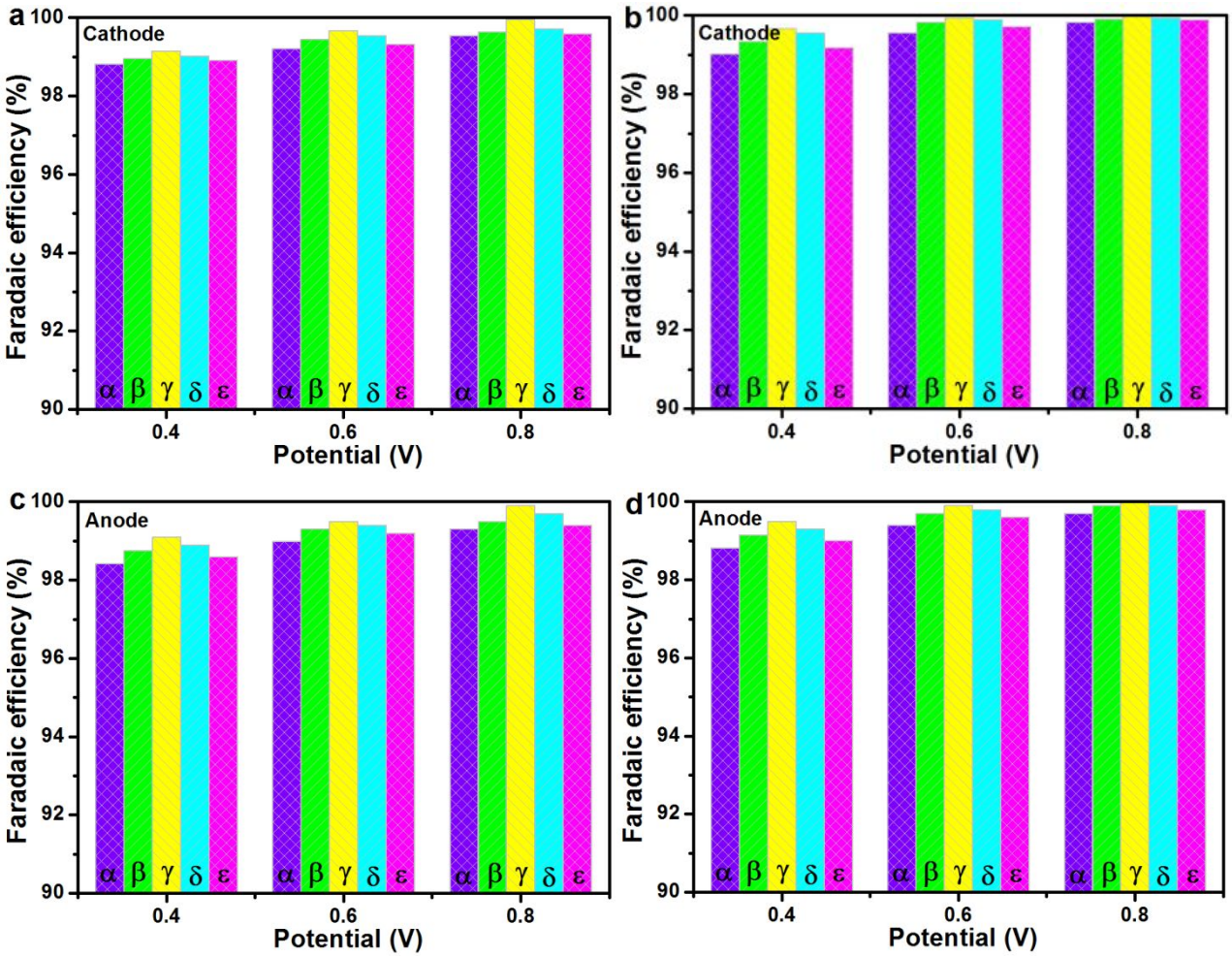

Figure S13. (**a**) The Faradaic efficiency for H_2 in cathode for electrochemical dehydrogenation of C_2H_6; (b) The Faradaic efficiency for CO/H_2 in cathode for electrochemical dehydrogenation of C_2H_6 in conjunction with CO_2 reduction in cathode; (c) The Faradaic efficiency for C_2H_4 production in anode for electrochemical dehydrogenation of C_2H_6; (**d**) The Faradaic efficiency for C_2H_4 production in anode for electrochemical dehydrogenation of C_2H_6 with CO_2 reduction. (α: Cu-NTMO, β: $Ni_{0.25}Cu_{0.75}$-NTMO, γ: $Ni_{0.5}Cu_{0.5}$-NTMO, δ: $Ni_{0.75}Cu_{0.25}$-NTMO, ε: Ni-NTMO).

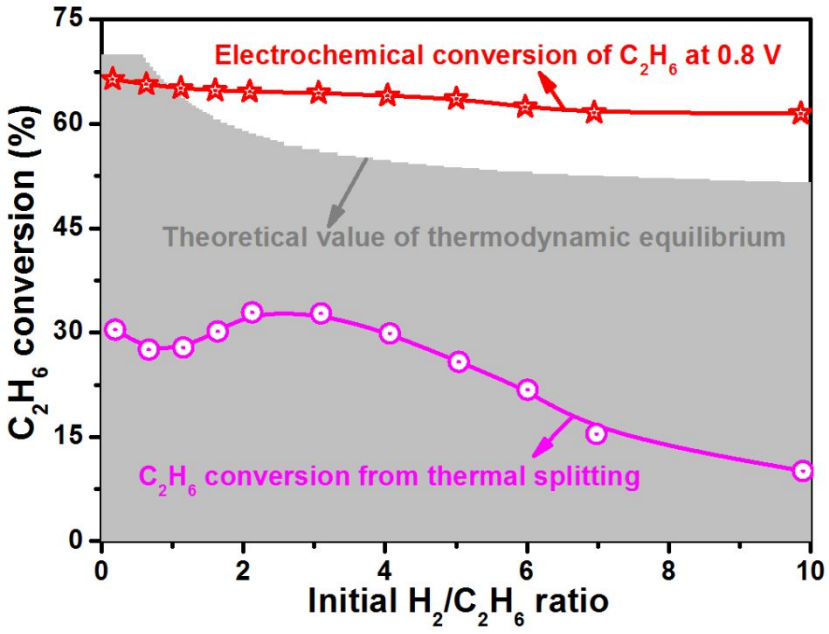

Figure S14 . The C_2H_6 conversion at different modes with $Ni_{0.5}Cu_{0.5}$-NTMO anode in solid oxide electrolyser.

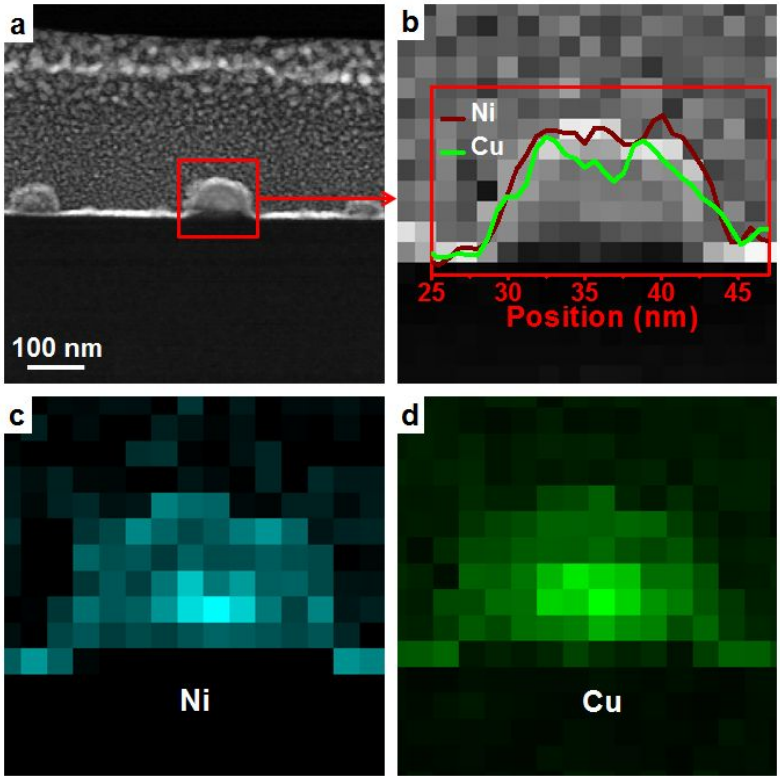

Figure S15. (a) The EDX mapping in HAADF-STEM mode of $Ni_{0.5}Cu_{0.5}$-NTMO anode after stability test for electrochemical dehydrogenation of C_2H_6; **(b)** EDX elemental line analysis across typical $Ni_{0.5}Cu_{0.5}$ particle; **(c, d)** Cu and Ni mapping of the exsolved nanoparticle.

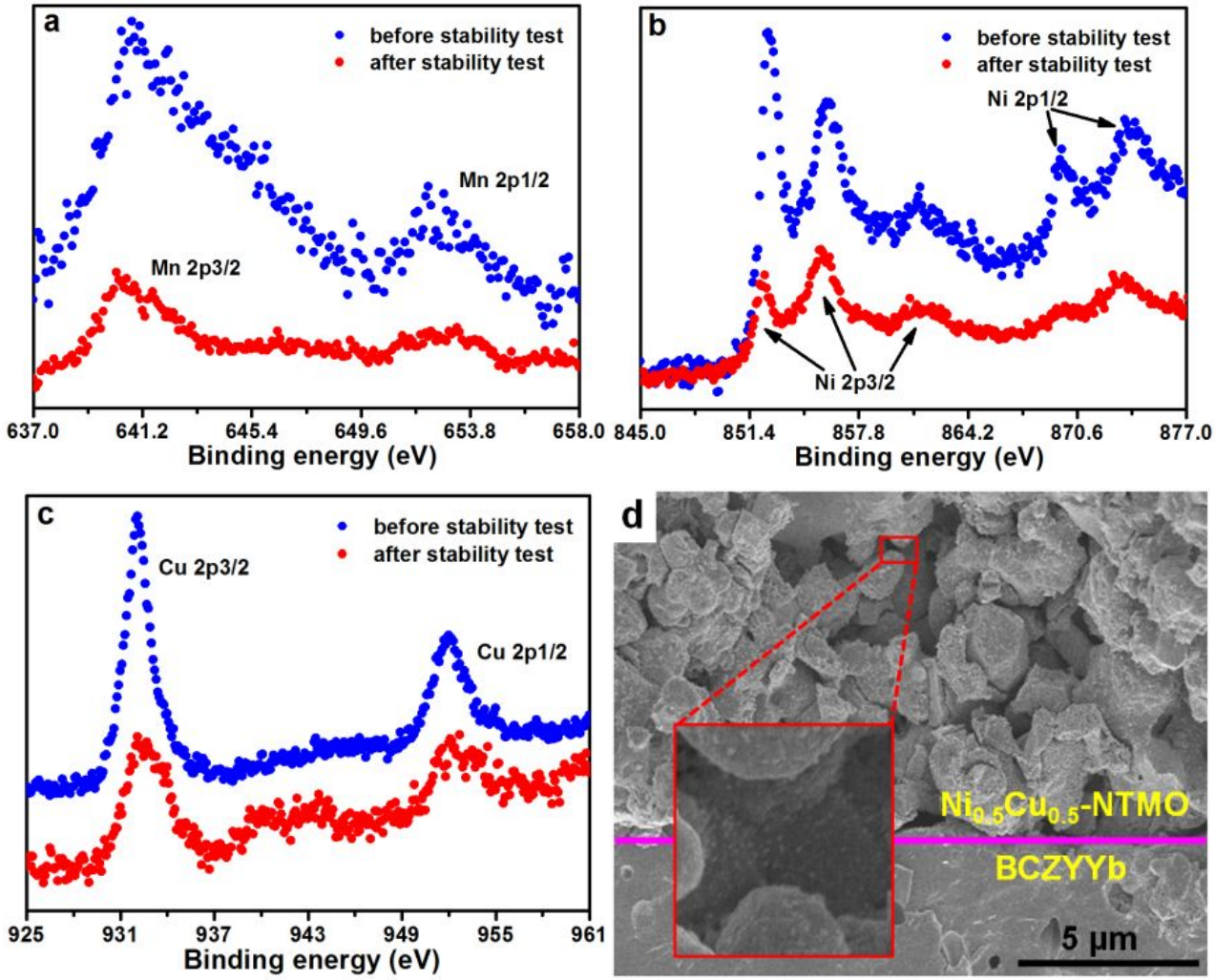

Figure S16. X-ray photoelectron spectroscopy of (a) Mn, (b) Ni, (c) Cu in $Ni_{0.5}Cu_{0.5}$-NTMO anode before and after stability test for electrochemical dehydrogenation of C_2H_6; (d) SEM images of the $Ni_{0.5}Cu_{0.5}$-NTMO porous electrodes after stability test for C_2H_6 conversion.

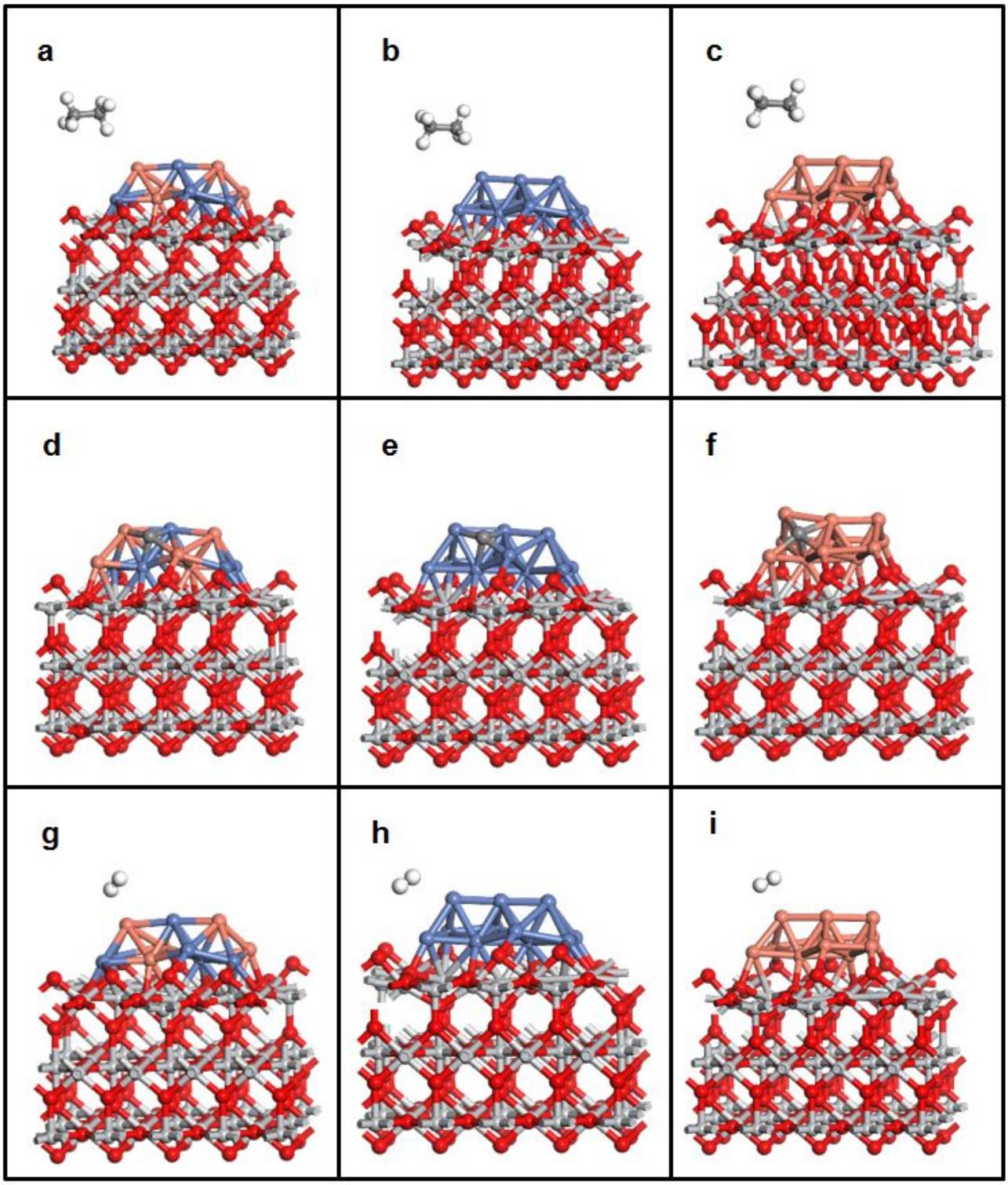

Figure S17. Optimized structure of ethane deep cracking process: (a-c) C_2H_6 (g) on cluster/TiO_2 system; (d-f) C adsorbed on cluster/TiO_2 system; (g-i) H_2 (g) on cluster/TiO_2 system. (a), (d) and (g): on (Ni-Cu)/TiO_2 system; (b), (e) and (h): on Ni/TiO_2 system; (c), (f) and (i): on Cu/TiO_2 system. (carbon in gray, copper in orange, nickel in bule, titanium in silver white, oxygen in red and hydrogen in white)

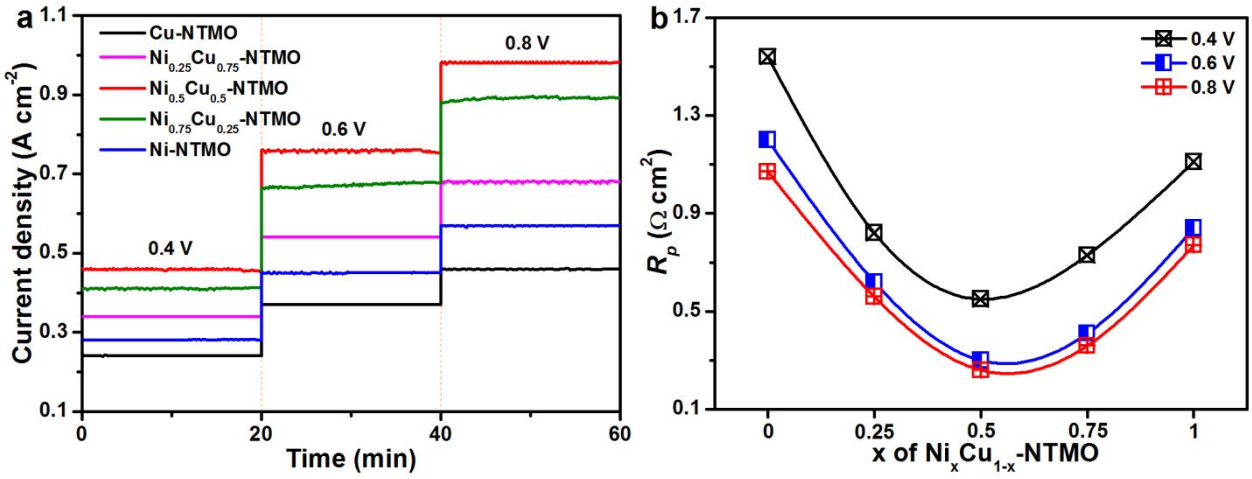

Figure S18. (**a**) The short-term operation of C_2H_6 dehydrogenation with the composite anodes in combination with CO_2 reduction at different voltages; (**b**) The electrode polarizations with different anodes at 0.4-0.8 V at 700 ˚C.

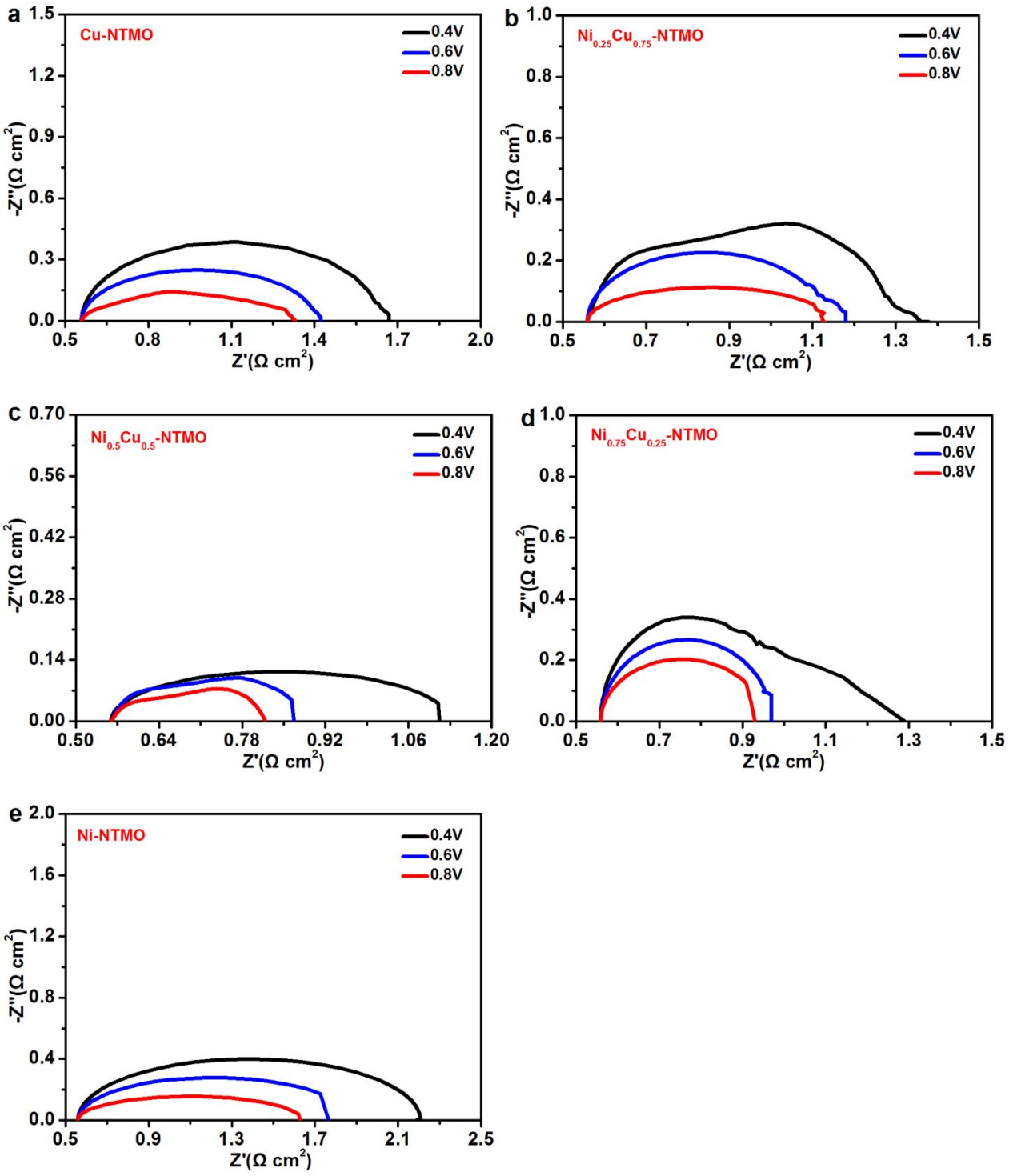

Figure S19. AC impedance of solid oxide electrolysers based on (a) Cu-NTMO, (b) $Ni_{0.25}Cu_{0.75}$-NTMO, (c) $Ni_{0.5}Cu_{0.5}$-NTMO, (d) $Ni_{0.75}Cu_{0.25}$-NTMO, (e) Ni-NTMO anodes under various potentials at 700 ˚C.

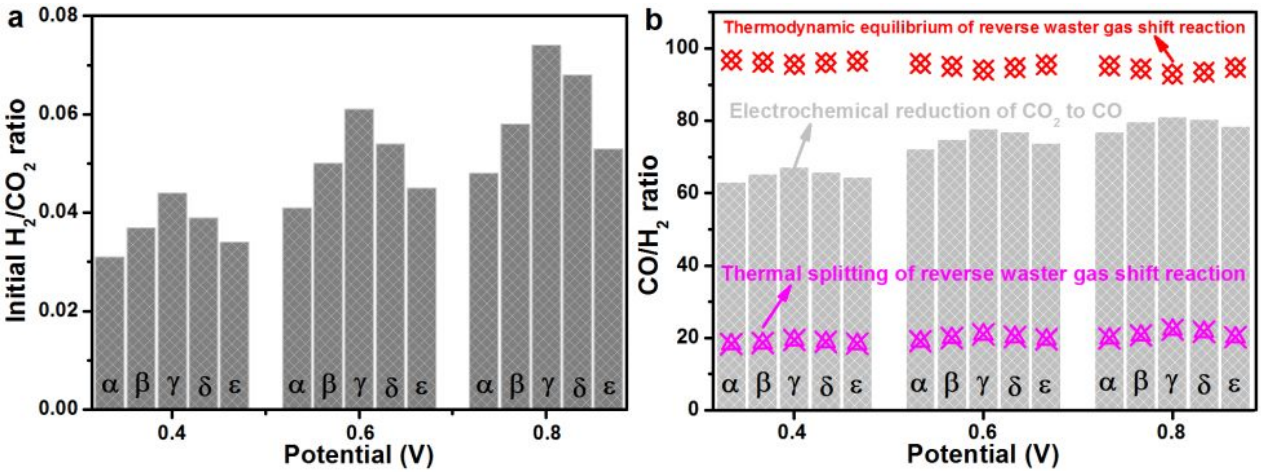

Figure S20. (a) Directly pumping the gas mixture of H_2/CO_2 to cathode under open circuit conditions, where the H_2 is identical to the H_2 generation amount in cathode during electrochemical C_2H_6 dehydrogenation; (b) the ratio of CO/H_2 at different modes in the cathode.

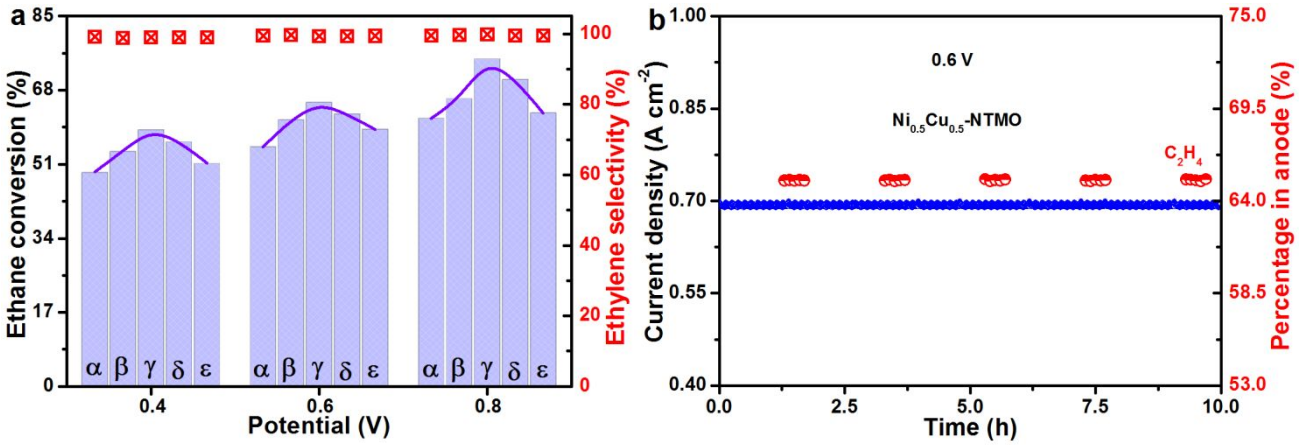

Figure S21. (**a**) C_2H_6 conversion and C_2H_4 selectivity in anode in combination with CO_2 reduction in cathode; (b) The short term performance of the electrochemical dehydrogenation of C_2H_6 with the $Ni_{0.5}Cu_{0.5}$-NTMO anode in a proton-conducting solid oxide electrolyser. (α: Cu-NTMO, β: $Ni_{0.25}Cu_{0.75}$-NTMO, γ: $Ni_{0.5}Cu_{0.5}$-NTMO, δ: $Ni_{0.75}Cu_{0.25}$-NTMO, ε: Ni-NTMO)